

## Critical evaluation of the light-scattering spectrum for single-particle excitations in *n*-GaAs at 300 K

D. A. Abramsohn,\* K. T. Tsen, and Ralph Bray

*Department of Physics, Purdue University, West Lafayette, Indiana 47907*

(Received 16 August 1982)

The line shape of the light-scattering spectrum for single-particle excitations in semiconductors such as *n*-GaAs has been commonly represented to be a simple Gaussian for a Maxwellian distribution of electrons. In this form it has been used as a probe of nonequilibrium populations of electrons. We present a critical evaluation of the adequacy of this approximation, based both on theory and on detailed, high-resolution measurements with Nd-doped yttrium aluminum garnet (Nd:YAlG) laser radiation at 1.06  $\mu\text{m}$  for a series of *n*-GaAs samples at 300 K, for concentrations in the range  $\sim 10^{13} < n < 10^{18}/\text{cm}^3$ . For low concentrations ( $n < 5 \times 10^{15}/\text{cm}^3$ ), we found a highly structured, competitive contribution to the spectrum from two-phonon-difference frequency combinations. This has to be subtracted from the measured spectrum to yield the single-particle contribution, and puts a lower limit of  $\sim 5 \times 10^{14}/\text{cm}^3$  on the electron populations that can be analyzed. Even for the corrected single-particle spectra, there are departures from a Gaussian line shape due to a variety of factors all inherent in the theory as formulated by Hamilton and McWhorter, but never fully analyzed or compared with experiment. These factors include band-structure effects (momentum dependence of the resonant enhancement term), overlapping contributions from Landau-damped plasmons, collisions, and a nonnegligible but always neglected zero-shift Compton-scattering term. The individual role and significance of these factors, as a function of carrier concentration, was determined from the theory and correlated with the experimental spectra. This analysis was carried out for the three scattering mechanisms associated with the charge-, energy-, and spin-density fluctuations of the solid-state electron plasma. We have found the spin-density fluctuation mechanism to be best suited to serve as a probe of electron distributions, but not without necessary corrections for the various experimental and theoretical factors.

### I. INTRODUCTION

There is a long history of research into the problem of light scattering, from electron plasmas, first in free space and more recently in crystals.<sup>1-12</sup> Light is scattered by both the single-particle and collective-mode excitations (plasmons) in the plasma, and also by coupled plasmon-phonon modes in the solid. The present work deals primarily with the contribution to the scattered-light spectrum from the single-particle excitations in a semiconductor, and includes inevitably some overlapping contributions from the plasmons. Our major interest is in a critical evaluation of the line shape of the single-particle-scattering (SPS) spectrum, including both the experimental problems of observing the spectrum against a background of competitive scattering contributions, and the theoretical problem of adequately expressing the form of the

spectrum. The latter is greatly complicated by the multiplicity of SPS mechanisms that can operate in the solid-state plasmas, and by the dependence of the light scattering on a host of factors, such as band structure, carrier concentration, and the collision frequency of the carriers. The theory of single-particle scattering has gone through a progressive development and evolution which has been described in a number of review articles.<sup>1-5</sup> For our purpose, we found the presentation of Hamilton and McWhorter<sup>7</sup> most useful, and our discussion will be based primarily on that formulation. The experimental side has no corresponding history of development. It is dominated by the pioneering and comprehensive work of Mooradian,<sup>2,8,9</sup> primarily on *n*-GaAs. Most of the subsequent work on SPS has dealt with various interesting special aspects which are outside the context of the present work.

The potential for the single-particle light-

scattering spectrum to serve as a probe of the properties of the electron plasma in a semiconductor was pointed out by Wolff.<sup>10,11</sup> The suggestion was implemented by Mooradian<sup>2,8,9</sup> in his extensive investigations of the spectrum in *n*-GaAs as a function of equilibrium electron concentration and temperature. The SPS spectrum has also been applied to the probing and analysis of nonequilibrium distributions of carriers, e.g., the departures from a Maxwellian distribution at high electric field in *n*-GaAs in the pre-Gunn-instability regime,<sup>12</sup> and for the measurement of the temperature of hot carriers generated by intense nonlinear Nd-doped yttrium aluminum garnet (Nd:YAlG) laser excitation.<sup>13</sup>

Common to all the probe studies of both equilibrium and nonequilibrium electron plasmas has been the representation of the SPS line shape as a Gaussian, centered at the laser line, for a Maxwellian distribution of carriers. Thus, the scattered-light intensity at a frequency shift  $\omega = \vec{q} \cdot \vec{v}$ , simply reflects the number of carriers with the same component of the velocity  $\vec{v}$ , in the direction of the wave vector transfer  $\vec{q}$ . The halfwidth of the spectrum provides a measure of the electron temperature. In the absence of screening effects, the integrated area of the Gaussian line is proportional to the electron concentration.

A Gaussian line shape follows quite readily for a collisionless, *free*-electron gas, where the scattering is due to the charge-density fluctuations in the plasma. Here, Salpeter<sup>14</sup> has shown that with increased electron concentration, the single-particle excitations are screened out, and eventually only the collective modes contribute to the scattering spectrum. At intermediate concentrations, where contributions from both excitations are present, the line shape is broadened by the overlapping Landau-damped plasmon, and departs strongly from the Gaussian form. The same thing happens in the solid-state plasma, but many new complications arise. The energy band structure of the material introduces several new factors. The scattering strength is greatly enhanced by the low effective mass of the electrons. There is an additional strong resonant enhancement factor for laser light close to the intrinsic absorption edge. The complexity of the energy band structure can introduce additional single-particle-scattering mechanisms,<sup>7</sup> the so-called spin-density and energy-density fluctuations, each with special features and quite different scattering strengths. It is apparent from the theory,<sup>3,7</sup> that there are several band-structure-related factors that can cause departures from a Gaussian line shape, and in a different manner for each of the scattering

mechanisms. Nevertheless, in the past, the single-particle spectrum has been deemed<sup>2,9</sup> to be adequately represented by a simple Gaussian line shape in *n*-GaAs at 300 K, even over the whole range of observable equilibrium electron concentrations ( $n \lesssim 10^{18}/\text{cm}^3$ ), and has been applied uncritically to the studies of nonequilibrium distributions.<sup>13</sup>

In the course of using the SPS spectrum as a probe of electrons excited from deep traps in *n*-GaAs by intense Nd:YAlG laser excitation,<sup>15</sup> we encountered a number of substantial discrepancies in this simple picture. This stimulated a reexamination of the line shape of the single-particle spectrum under equilibrium conditions. This investigation, carried out at 300 K in a series of *n*-GaAs samples ranging in concentration from  $< 10^{13}/\text{cm}^3$  to  $\sim 10^{18}/\text{cm}^3$ , is the main subject of this paper.

For perspective, we summarize below the major factors which we found to contribute to the complication of the SPS line shape and to affect its usefulness as a probe: (1) A hitherto unreported residual contribution from two-phonon scattering appears close to the laser line and begins to compete with SPS for carrier concentrations  $n \leq 10^{15}/\text{cm}^3$ . The lattice contribution must be subtracted from the spectrum if the SPS contribution is to be properly analyzed. (2) For the dominant, charge-density-fluctuation mechanisms of light scattering, the line shape deviates significantly from a Gaussian with the onset of screening of the single-particle excitations and growth of a Landau-damped plasmon contribution at  $n > 10^{15}/\text{cm}^3$ . (3) There is a considerable resonant enhancement of the single-particle scattering for Nd:YAlG laser light at 1.17 eV. The  $\vec{k}$  dependence of this resonant factor can give substantial deviations from a Gaussian line shape. (4) Collisions can strongly affect the SPS line shape, and greatly enhance the damping of any relevant plasmon contribution.

Although many of the reasons for the departures from a Gaussian line shape (items 2, 3, and 4 above) are implicit in the theory of Hamilton and McWhorter,<sup>7</sup> the analysis of the latter has never been presented in detail, either alone or in conjunction with experimental data. Rather, simplifying assumptions or approximations have been made which permitted a Gaussian line shape to emerge. In Sec. II, we shall analyze the theory in such a way as to isolate the several factors that induce departures from a Gaussian line shape, and determine the specific significance of each factor.

Our analysis of the theory does not directly include the effects of collisions. A complementary study of the effects of collisions only has been car-

ried out by Hertel and Appel,<sup>16</sup> and applied to some of our data. It omits the complications due to band structure included in this paper, and is restricted to the charge-density-scattering mechanism. It goes beyond existing theory by taking into account the energy dependence of the collision time, due to impurity- and lattice-scattering mechanisms in *n*-GaAs. We shall call on their results to supplement the analysis of competitive two-phonon scattering and band-structure effects which are central to our work. Although, in principle, the combined effects of collisions and band-structure effects on the line shape can be carried out for the various light-scattering mechanisms, such an analysis would be extremely complicated, and tend to obscure the role of the individual factors.

In Sec. III, we shall describe the experimental setup. Our use of a computer to control the scanning, recording, and storage of the data permitted long extended runs and analyses which helped to yield many of the new details not reported in the older investigations. A comprehensive survey of the experimental results will be given in Sec. IV. The discussion of these results will illustrate the role of the three different single-particle-scattering mechanisms in the evolution of the SPS line shape. We shall make use of the insight gained by the separate analysis of the effects of collisions, to discuss qualitatively what further influence they have on the line shape. Finally, we shall comment on the optimal conditions for employing SPS as a probe of non-equilibrium populations of electrons, and warn against errors made in its previous use for that purpose.

## II. THEORY

The light-scattering spectrum for single-particle excitations in *n*-GaAs at 300 K lies in a broad continuum of  $\sim 100 \text{ cm}^{-1}$  on both sides of the laser line. It can be generated by three different scattering mechanisms which have different scattering strengths and some differences in line shape. These scattering mechanisms have been ascribed to charge-density fluctuations (CDF), spin-density fluctuations (SDF), and energy-density fluctuations (EDF). The conditions under which each can appear, and the differences in the line shapes, will be made clear from the comprehensive theoretical expression for the scattering cross section to be presented later in this section. However, we shall first present the common expression to which they all reduce and conform if certain approximations

(to be specified later for each scattering mechanism) are made. This common form represents the "simple" Gaussian line shape.

### A. The Gaussian line shape

When a Gaussian line shape is an adequate approximation for a Maxwellian distribution of carriers with infinite collision time, then the differential cross section for Stokes scattering by single-particle excitations of frequency  $\omega$  and wavevector  $\vec{q}$  can be represented<sup>5</sup> by

$$\frac{d^2\sigma}{d\Omega d\omega} \propto \frac{\omega_i}{\omega_s} R_0^2 \left[ \frac{E_G^2}{E_G^2 - (\hbar\omega_i)^2} \right]^2 \frac{n}{qv_{\text{th}}} \times \exp \left[ -\frac{(\omega - \omega_c)^2}{(qv_{\text{th}})^2} \right], \quad (1)$$

where  $\omega_i$  and  $\omega_s$  are the incident and scattering frequencies,  $v_{\text{th}} = (2k_B T/m^*)^{1/2}$  is the thermal velocity of the electrons,  $m^*$  is the effective mass, and  $R_0^2 = (e^2/m^*c^2)^2$  is the Thomson cross section. The exponential term represents a Gaussian, shifted slightly from the laser line by  $\omega_c = \hbar q^2/2m^*$ . The latter arises in the expression for the frequency shift due to scattering from electrons,  $\omega = \vec{q} \cdot \vec{v} - \hbar q^2/2m^*$ , and it represents the Compton shift for scattering by electrons with zero velocity in the direction of wave-vector transfer  $\vec{q}$ . This zero shift is generally neglected; however, it is nearly  $4 \text{ cm}^{-1}$  for electrons with the small effective-mass ratio of 0.067 in GaAs, and is not insignificant. It will be retained in all further references to the simple Gaussian line shape. The band-structure effects are represented in Eq. (1) by the inclusion of an effective mass and the resonant enhancement term (the squared term in parentheses). The form of the latter is simplified here to include a single energy gap  $E_G$ , evaluated at  $k=0$ . The combination of band-structure factors enhances the strength of the single-particle scattering by a factor of  $\sim 2000$ , for  $\hbar\omega = 1.17 \text{ eV}$ . The height or area of the Gaussian line is proportional to the total electron concentration  $n$ .

As is evident, the electron temperature can be obtained from the halfwidth of the Gaussian. It is less evident that the temperature can also be obtained from the ratio of Stokes to anti-Stokes scattering strengths. The anti-Stokes spectrum is

obtained by replacing  $\omega$  by  $-\omega$  in Eq. (1). The Stokes to anti-Stokes ratio then reduces to  $e^{\hbar\omega/k_B T}$  which is equivalent to  $[\tilde{n}(\omega) + 1]/\tilde{n}(\omega)$ , where  $\tilde{n}(\omega)$  is the Bose-Einstein factor. It should be noted that it is important to retain the Compton shift  $\omega_c$ , both to give the correct Stokes to anti-Stokes ratio, and to give the zero shift of the Gaussian away from the laser line. The generally made approximation<sup>5</sup> of neglecting  $\omega_c$  and replacing  $[\tilde{n}(\omega) + 1]$  by  $k_B T/\hbar\omega$  if the latter is  $\gg 1$ , obscures these significant points.

### B. Departures from a Gaussian line shape

For the more complete analysis, we follow the theory as presented by Hamilton and McWhorter. It serves admirably for a description of the origin and role of the different light-scattering mechanisms, the effects of band structure and the evolution of the line shape with change in carrier concentration. From Eqs. (17) and (18) of Hamilton and McWhorter,<sup>7</sup> and with a slight rearrangement of terms, we obtain

$$\frac{d^2\sigma}{d\Omega d\omega} = \frac{\omega_s}{\omega_i} \left[ \frac{e^2}{mc^2} \right]^2 \frac{\hbar}{\pi} \frac{1}{1 - e^{-\hbar\omega/k_B T}} \text{Im} \left[ \left( \frac{L_2}{1 + L_0/F} + \frac{L_0/F}{1 + L_0/F} (L_2 - L_1^2/L_0) \right) (\hat{e}_i \cdot \hat{e}_s)^2 + K_2 (\hat{e}_i \times \hat{e}_s)^2 \right], \quad (2)$$

where  $\hat{e}_i$  and  $\hat{e}_s$  are the incident and scattered polarization vectors,  $F = \epsilon(\omega)q^2/4\pi e^2$ , and  $\epsilon(\omega)$  is the longitudinal dielectric constant of the lattice, given by  $\epsilon_\infty [1 + (\omega_l^2 - \omega_t^2)/(\omega_t^2 - \omega^2)]$ ;  $\omega_l$  and  $\omega_t$  are the frequencies of the longitudinal- and transverse-optical phonons, and  $\epsilon_\infty$  is the optical dielectric constant. Also

$$\left\{ \frac{L_n}{K_n} \right\} = \frac{2}{(2\pi)^3} \int d^3k \frac{\vec{v} \cdot \vec{q} \frac{\partial f}{\partial \epsilon}}{\omega - \vec{v} \cdot \vec{q} - \frac{\hbar q^2}{2m^*}} \times \left\{ \begin{matrix} A_{\vec{k}}^n \\ B_{\vec{k}}^n \end{matrix} \right\}, \quad (3)$$

where  $f$  is the distribution function of the electrons. The band-structure complications are included in the terms  $A_{\vec{k}}$  and  $B_{\vec{k}}$ , which are given by

$$A_{\vec{k}} \equiv \left[ 1 + \frac{P^2}{m} \left( \frac{E_{G_1}}{E_{G_1}^2 - (\hbar\omega_i)^2} + \frac{(\frac{1}{3})E_{G_2}}{E_{G_2}^2 - (\hbar\omega_i)^2} + \frac{(\frac{2}{3})E_{G_3}}{E_{G_3}^2 - (\hbar\omega_i)^2} \right) \right], \quad (4)$$

$$B_{\vec{k}} \equiv \left[ \frac{2P^2}{3m} \right] \left[ \frac{\hbar\omega_i}{E_{G_2}^2 - (\hbar\omega_i)^2} - \frac{\hbar\omega_i}{E_{G_3}^2 - (\hbar\omega_i)^2} \right]. \quad (5)$$

Here,  $E_{G_i}$  is the energy difference between the conduction band and the  $i$ th valence band, evaluated at wave vector  $\vec{k}$ , and  $P \equiv -i \langle s | P_z | z \rangle$  is the inter-band matrix element of the momentum.

The theory, as presented above, includes in addition to the approximations made by Hamilton and McWhorter the following simplifications: As noted before, we have neglected collisions in the expressions for  $L_n, K_n$ . We have also dropped an anisotropic term (the  $\hat{p}\hat{p}$  term in  $A_{\vec{k}}$  and  $B_{\vec{k}}$ ), whose contribution is minor in most situations of interest. In evaluating the  $\vec{k}$ -dependent terms in  $A_{\vec{k}}$  and  $B_{\vec{k}}$ , we have used the effective-mass ratio 0.067 for electrons, and effective hole masses<sup>17</sup>:  $m_1^* = 0.68m$ ,  $m_2^* = 0.12m$ , and  $m_3^* = 0.20m$ . We took

$E_{G_1} = E_{G_2} = 1.43$  eV at  $k=0$ , and  $\Delta = 0.33$  eV, and assumed parabolic bands with spherical energy surfaces.

The different scattering mechanisms for single-particle excitations are related to specific terms in Eq. (2). The two terms in the large parentheses associated with  $(\hat{e}_i \cdot \hat{e}_s)^2$  relate to the charge-density and energy-density fluctuation mechanisms, respectively. The term associated with  $(\hat{e}_i \times \hat{e}_s)^2$  relates to the spin-density-fluctuation mechanism.

The relative magnitudes of these three mechanisms are strongly dependent on the band-structure terms  $A_{\vec{k}}, B_{\vec{k}}$ , responsible for resonant enhancement. In the absence of screening (i.e.,  $L_0/F \ll 1$ ), the ratio  $A_{\vec{k}}$  to  $B_{\vec{k}}$  and hence the ratio

$\text{Im}L_2/\text{Im}K_2$ , determines the relative magnitude of the CDF and SDF scattering mechanisms. This ratio<sup>7</sup> is 32.4 for *n*-GaAs at 300 K.

The  $\vec{k}$  dependence of  $A_{\vec{k}}$  and  $B_{\vec{k}}$  is of special interest. If the  $\vec{k}$  dependence is neglected in  $A_{\vec{k}}$ , then the term  $(L_2 - L_1^2/L_0)$  goes to zero,<sup>11</sup> and the EDF mechanism vanishes. Furthermore, with the  $\vec{k}$  dependence of  $A_{\vec{k}}$  and  $B_{\vec{k}}$  neglected, the integrals  $L_2$  and  $K_2$  over the electron distribution in  $\vec{k}$  space yield a Gaussian line shape, as given in Eq. (1). The magnitude of the departure from a Gaussian, due to the inclusion of the  $A_{\vec{k}}$  and  $B_{\vec{k}}$  in the integrals, will be analyzed later.

Screening has an important effect on the scattering mechanisms and on the line shape. The strength of the screening is embodied in the factor  $L_0/F$ , or equivalently  $(q_D/q)^2$ , where  $q_D$  is the Debye wave vector, given by  $4\pi ne^2/k_B T\epsilon_\omega$ . Screening plays no role for the SDF mechanism.<sup>2,7</sup> The strength of the latter is determined by  $\text{Im}K_2$ , and is linearly proportional to *n*. For the CDF mechanism, screening is negligible at low carrier concentration, such that  $L_0/F \ll 1$ , and then only the single-particle excitations contribute to the spectrum. Their contribution, as determined by  $\text{Im}L_2$ , increases linearly with *n*. However, as  $(q_D/q)^2$  approaches 1 at  $n \sim 10^{16}/\text{cm}^3$  in *n*-GaAs at 300 K, the screening becomes important<sup>9</sup>; the single-particle-scattering contribution reaches a peak and then decreases with further increase in *n*. Coincident with the onset of screening, the plasmon contribution becomes noticeable. At an early stage, it is so strongly Landau damped that it does not affect the line shape. However, as the screening of the single-particle contribution increases, the two contributions are mingled, giving rise to a very broadened spectrum. Eventually, as the single-particle spectrum diminishes, the plasmon contribution takes the form of distinguishable Stokes and anti-Stokes peaks at a frequency shift corresponding to the plasma frequency.

With the screening out of the CDF contribution to the single-particle spectrum, the EDF contribution takes over. As  $L_0/F$  becomes large, the coefficient of the factor  $L_2 - L_1^2/L_0$  becomes unity, so that the EDF mechanism is not subject to screening. It is responsible for the maintenance of the single-particle spectrum centered at the laser line. The EDF mechanism has been shown<sup>2</sup> to vanish at low temperature and to increase and become important only at high temperatures.

We shall now proceed to illustrate what happens to the line shape of the single-particle spectrum, as

we progressively take into account the various factors in Eq. (2). We consider first the case for the polarization configuration  $(\hat{e}_i || \hat{e}_s)$ . The analysis is illustrated in Figs. 1(a)–1(e) for progressively increasing electron concentrations, from  $5 \times 10^{14}/\text{cm}^3$  to  $1 \times 10^{17}/\text{cm}^3$ . For each carrier concentration, we plot four curves with contents described below.

Curve 1 contains the  $L_2$  term only, with the  $\vec{k}$  dependence of  $A_{\vec{k}}$  neglected. The resonant enhancement term now can be taken outside the integral over the distribution function, and the line shape is the simple (zero-shift) Gaussian for a Maxwellian distribution. Curve 2 contains the  $L_2$  term but with the  $\vec{k}$  dependence of  $A_{\vec{k}}$  included. The effect of the latter is to give a narrowing of the halfwidth of the Gaussian by  $\sim 10\%$  in GaAs at 300 K. The effect of  $A_{\vec{k}}$  is obviously enhanced the closer the incident photon energy is to the energy gap. Curve 3 contains the term  $L_2/(1 + L_0/F)$ , i.e., the full CDF contribution. This term shows the effect of screening in decreasing the SPS contribution, and in being simultaneously responsible for the onset of the plasmon contribution. The decrease in the SPS contribution is already appreciable at  $n = 5 \times 10^{15}/\text{cm}^3$ . The plasmon contribution is very broad due to strong Landau damping when the plasmon frequency is still very close to the laser line and overlaps the SPS contribution. It manifests itself initially as a bulging in the SPS spectrum. With increasing carrier concentration, the SPS contribution progressively diminishes due to screening, and the plasmon contribution moves out to the wings of the SPS contribution, where it finally generates its own distinctive Stokes and anti-Stokes peaks. Curve 4 contains the full  $(\hat{e}_i \cdot \hat{e}_s)^2$  term, which includes the EDF as well as the CDF contribution. It shows the restoration of the SPS contribution in the central symmetric peak, which grows with increasing carrier concentration. To better demonstrate this, we have replotted curves 3 and 4 on an expanded scale in Figs. 1(c'), 1(d'), and 1(e').

For the SDF mechanism, governed by the  $(\hat{e}_i \times \hat{e}_s)^2$  term, the transition in line shape is much simpler since there are no interactions with plasmons. With the  $\vec{k}$  dependence of the  $B_{\vec{k}}$  term neglected, the line shape is the simple (zero-shift) Gaussian. Inclusion of the  $\vec{k}$  dependence in the resonant enhancement terms gives a larger effect than for the CDF case. There is now an appreciable 20% narrowing of the halfwidth. The resultant line shapes are illustrated in Fig. 2. The three normalized curves provide a comparison of (a) the simple, zero-shift Gaussian, and the narrowed lines for (b)

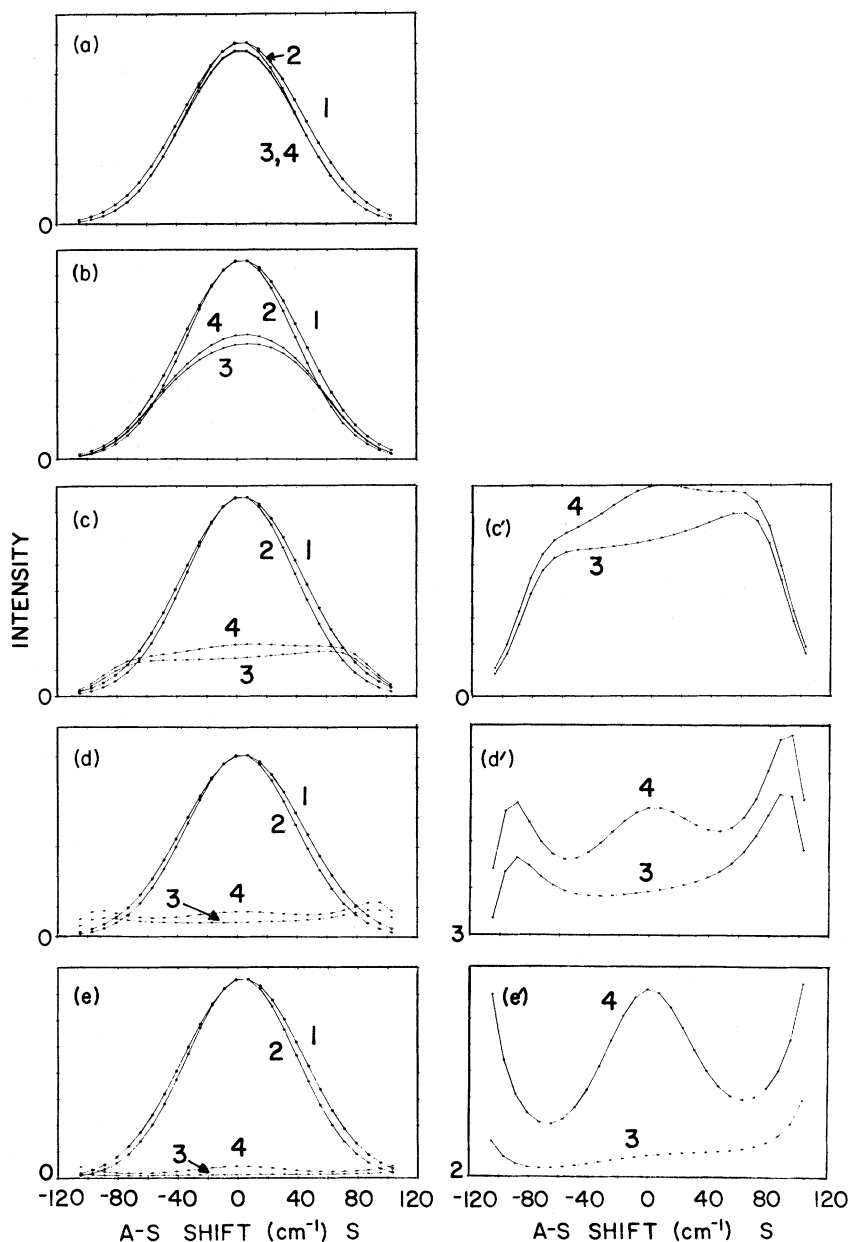


FIG. 1. Theoretical single-particle spectra based on Eq. (2) for collisionless case, for the charge-density- and energy-density-fluctuation mechanisms, corresponding to  $(\hat{e}_i || \hat{e}_s)$ . Carrier concentrations are (a)  $5 \times 10^{14}/\text{cm}^3$ , (b)  $5 \times 10^{15}/\text{cm}^3$ , (c)  $2 \times 10^{16}/\text{cm}^3$ , (d)  $4 \times 10^{16}/\text{cm}^3$ , and (e)  $1 \times 10^{17}/\text{cm}^3$ . Curves 1 to 4 (see text) represent successively better approximations in analysis of Eq. (2). Curves 3 and 4 are shown enlarged in (c')–(e') to demonstrate the growing contribution of the EDF mechanism in curve 4. [Note the change in zero levels in (d') and (e').]

the CDF and (c) the SDF mechanisms due to the  $\vec{k}$ -dependent  $A_{\vec{k}}$  and  $B_{\vec{k}}$  terms, respectively.

The main effect of collisions in the CDF scattering regime is on the plasmon contribution. Collisions contribute strongly to the damping of the plasmon. In the  $(10^{15} - 10^{16})/\text{cm}^3$  range of electron concentration, the line shape of the combined, over-

lapping SPS and plasmon contributions is very sensitive to collision frequency, and therefore extremely difficult to use for a probe of the electron plasma. This is illustrated in Fig. 3 by a set of theoretical curves at  $n = 6 \times 10^{15}/\text{cm}^3$  for a range of collision times, as calculated by Hertel and Appel<sup>16</sup> for constant  $\tau$ . The band-structure complications have

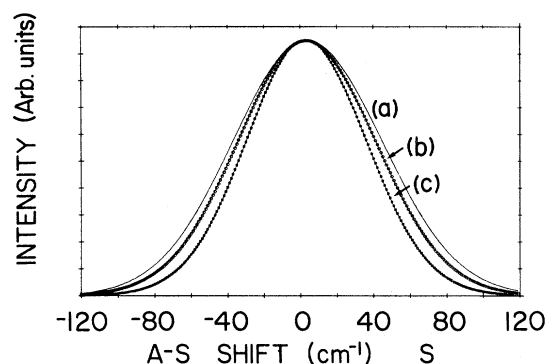


FIG. 2. Theoretical line shapes comparing single-particle spectra (collisionless case) for (a) the (zero-shift) Gaussian, (b) the effect of the inclusion of the  $\vec{k}$  dependence of the  $A_{\vec{k}}$  term for the CDF mechanism, and (c) the effect of the inclusion of the  $\vec{k}$  dependence of the  $B_{\vec{k}}$  term for the SDF mechanism.

been neglected in these theoretical curves, but they are not particularly significant in this regime. It is evident that the effect of decreasing  $\tau$  is to reduce the plasmon bulging of the spectrum and to tend to restore the narrower SPS line shape. At the shortest  $\tau$  in Fig. 3, the plasmon contribution is completely damped and the SPS spectrum has evolved into a narrowed, Lorentzian-type form. However, it should be noted that short collision times are associated in *n*-GaAs at 300 K, with very high impurity concentration, and depending on the compensation, high carrier concentration. High carrier concentration will screen out the single-particle spectrum for the CDF mechanism, and its line shape will be irrelevant. The transition from a Gaussian to a

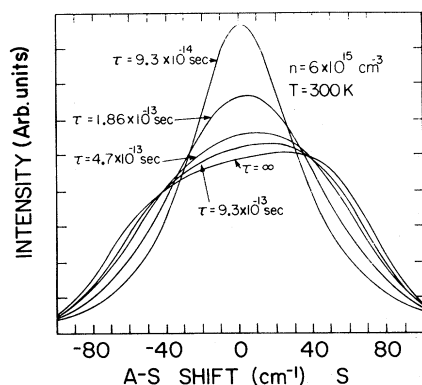


FIG. 3. Demonstration of effect of energy-independent collision time on the single-particle spectrum for the charge-density-fluctuation mechanism [after Hertel and Appel (Ref. 16)].

Lorentzian line shape with decreasing  $\tau$  is perhaps more relevant for the EDF and SDF mechanisms which are not screened out at high carrier concentration. In the simplified case that band-structure complications are neglected, it can be shown that such a transition does occur for the latter case. Nevertheless, at high carrier concentrations,  $n > 10^{17}/\text{cm}^3$ , other effects such as departure from a Maxwellian distribution, nonparabolicity in the conduction band and band tailing, can also become significant and complicate the analysis. Thus a clean test for the more extreme effects of collision damping on the SPS line shape may not be feasible in *n*-GaAs, and may be better left for relatively pure materials with much lower values of mobility and collision times, e.g., CdS.

We summarize the conditions under which the simple Gaussian line shape can be applicable: (i) The carriers have a Maxwellian distribution in a parabolic band, (ii) the  $\vec{k}$  dependence of resonant enhancement factors  $A_{\vec{k}}$  and  $B_{\vec{k}}$  can be neglected, or measurements can be made sufficiently far from the absorption edge that the resonant enhancement is not involved, (iii) for the CDF mechanism,  $(q_D/q)^2 \ll 1$ , so that screening is negligible and there is no distortion of the line shape by the overlapping plasmon contribution, and (iv) the collision time is sufficiently large. Furthermore, the Compton-shift term can be ignored only if the effective-mass ratio of the carriers is not too small.

From the discussion of the various theoretical factors which can complicate the line shape for the SPS, we can conclude that the use of SPS as a probe is best accomplished for the SDF mechanism. Only for this mechanism is the magnitude of the spectrum linear with carrier concentration and the line shape not dependent on  $n$ , at least in the absence of collisions. The much stronger CDF mechanism can be employed only for a very restricted range of carrier concentration, when the plasmon contribution can be ignored. The experimental test of these conclusions, as well as the role of other factors affecting the scattering spectrum, will be considered in Sec. IV.

### III. EXPERIMENTAL ARRANGEMENT AND DETAILS

#### A. General features

The Raman scattering measurements were made with a Nd:YAlG laser ( $1.0641 \mu\text{m}$ ) which could be operated in the cw or Q-switched mode. Since

GaAs is only weakly absorbing at this wavelength, the laser beam is substantially transmitted through samples  $\sim 0.3$ -cm long. The light scattered at  $90^\circ$  was analyzed by a stepped Spex Model 1402 0.85-m double monochromator equipped with two 1200-groove/mm gratings blazed at  $1\text{ }\mu\text{m}$ , and silvered optics. With the three slits set at 1.0 mm for all scans, the spectral resolution is  $3.65\text{ cm}^{-1}$  at  $1.06\text{ }\mu\text{m}$ . The stepper drive was used to take measurements at  $1\text{-}\text{\AA}$  intervals. An RCA 7102 photomultiplier with *S*-1 response, cooled to  $\sim -95^\circ\text{C}$  was used in a photon-counting mode. The cooling, together with a magnetic defocusing assembly in the shielded housing, gave a dark count of less than 1 count per second at the discriminator level setting chosen to reject false "counts" generated by the laser power supply and the temperature controller for the photomultiplier housing. For *Q*-switched measurements, a 60-nsec gate, centered on the 100-nsec, *Q*-switched pulse, was used in the scaler circuit.

A General Automation minicomputer (Model spc 16/40) was employed for controlling the scanning, and for the taking, storage, and processing of the data. The computer was also used to flip an optical attenuator in front of the exit slit when the monochromator was scanning through the laser line, and to receive monitoring data on the sample temperature (from a thermocouple attached to the sample) and on the light intensity transmitted through the sample to a power meter. With these controls, runs lasting several days could be facilitated when necessary. Output information from the computer was observed on an oscilloscope and recorded with a digital plotter. The ability of this system to obtain, correct, and record Raman data in great detail was essential for the detection and study of various subtle features in the SPS line shape which had been overlooked in previous studies.

### B. Stray-light effects

For measurements in the single-particle-scattering continuum, to within  $\sim 10\text{ cm}^{-1}$  of the laser line, it was crucial to minimize the parasitically scattered light. We found that much of the latter appeared to originate as diffuse scattering from the points of entry and exit of the laser beam on the sample, and from the edges and corners of the sample. We devised a sample mount with shields to block most of these contributions. A 1-mm pinhole, located 1 mm from the corner of the sample was used to permit only the central portion of

the focused laser beam to be incident on the sample. The shielding extended also on the scattered side to mask both sample ends and all but a 2-mm central region of the sample from the monochromator.

A source of early difficulty for measurements on samples with the lowest carrier concentration, was extraneous light reaching the spectrometer and the detection system. A Baird-Atomic N-900 filter mounted directly at the entrance slit of the monochromator served as a filter to cut off wavelengths below  $9060\text{ \AA}$  and eliminate all second-order contributions from visible light in the darkened room. A more serious problem was from stray radiation from the laser cavity, including that from the krypton pump lamp. All diffusely scattered light was eliminated by carefully enclosing the laser. However, some radiation still persisted that was collinear with the laser beam. This source and the contributions from gratings ghosts in the spectrometer were carefully examined for a variety of different scattering sources, including light directly scattered into the spectrometer from a metal needle and from diffuse reflectors. It could be ascertained that the level of all such contributions fell well below the Raman-scattered contributions even from our purest GaAs samples. The undesired light could be identified by its lack of the symmetric Stokes and anti-Stokes structure characteristic of Raman-scattered light. Thus, the grating ghosts reported by Mooradian<sup>9</sup> as affecting results for his purest samples, were determined to be absent in all the measurements reported here. On the contrary, an important residual contribution was discovered from two-phonon scattering in GaAs, which had to be taken into account before the scattering contribution from single-particle excitations could be analyzed.

### C. Data handling, calibration, and normalization

The spectral response of the whole Raman system was calibrated with a known spectral source (a tungsten ribbon filament lamp). This calibration was stored in the computer and used to correct all Raman scattering data for instrumental response. The data were also normalized for fluctuations in the laser intensity. All the data reported here were subjected to a double binomial smoothing. Generally, each spectrum was scanned very slowly, repeated at least twice, and then averaged if each scan was seen to be free of artifacts. Baseline subtractions were made for dark-count background and (on only one sample) for a fluorescent background.



It was also necessary to normalize for the actual amount of laser light in the scattering volume which is imaged on the cathode of the photomultiplier. This was accomplished by dividing each spectrum point by point, by the intensity of the Stokes TO-phonon line (represented by its integrated area) obtained during the same scan. Thus when spectra for different runs and different samples are processed in this fashion and plotted to the same scale, the data represent only differences in scattering strengths. All these precautions and procedures were essential for subtraction of lattice-scattering contributions on samples with negligible single-particle-scattering contributions, from other samples with appreciable electronic contributions, and finally for comparing the electronic-scattering contributions on samples with different carrier concentrations.

#### D. Crystal orientation and scattering configuration

It was very important in the analysis of the Raman scattering data to carefully control the scattering configuration in order to appropriately separate and distinguish the contributions from the different excitations in the sample. This required strict adherence to selection rules, careful orientation of samples, and control of the polarization of the incident and scattered light. All the scattering data reported here were taken with the laser beam entering the sample in the  $[110]$  direction and with the scattered light collected at  $90^\circ$  in the  $[1\bar{1}2]$  direction. Measurements were always made for both the  $(\perp\text{--}\perp)$  and  $(\parallel\text{--}\perp)$  scattering configurations, where the symbols refer to polarization of the incident and scattered light respectively, with respect to the plane of scattering. The  $(\perp\text{--}\perp)$  or  $\hat{e}_i\parallel\hat{e}_s$  configuration corresponds to single-particle scattering by the CDF and EDF mechanisms, and  $(\parallel\text{--}\perp)$  or  $\hat{e}_i\perp\hat{e}_s$  to the SDF mechanism. For the phonon-scattering contributions,  $\hat{e}_i\parallel\hat{e}_s$  corresponds to  $\Gamma_1+\Gamma_{15}$  symmetry with scattering strength given by  $a^2+\frac{4}{3}d^2$  in the notation of Loudon<sup>18</sup>; the  $\hat{e}_i\perp\hat{e}_s$  case corresponds to  $\Gamma_{12}+\Gamma_{15}$  with  $2b^2+\frac{1}{3}d^2$  scattering strength. In general, the  $\hat{e}_i\parallel\hat{e}_s$  configuration gives much stronger scattering for both the electronic and lattice excitations. It has been established<sup>19</sup> that for two-phonon-scattering contributions, the  $\Gamma_1$ -scattering contribution is predominantly due to overtones (two phonons with the same frequency and opposite wave vectors), where  $\Gamma_{15}$  scattering is predominantly due to combinations (two phonons

with different frequencies, in different branches, and with opposite wave vectors). The  $\Gamma_{12}$  contribution to the spectrum is generally negligible.

Particular care was essential for maintaining the polarization of the light. The polarizer inside the laser cavity was found insufficient to guarantee the desired degree of polarization of light entering the sample, especially after several reflections from mirrors. It was therefore supplemented with a Glan-laser polarizer which was used as the last optical element preceding the sample. The analyzer for the scattered light was a 2-in. square of Polaroid (HR8) with rejection ratio of 920:1 and 72% throughput of the desired component. It was placed as the first optical element to be encountered by the scattered light and works well even with non-normal light incident on it. The latter point is important because the scattered light was collected at an angle of up to  $22^\circ$  from the normal (which corresponds to a  $6.1^\circ$  half-angle inside the GaAs sample with refractive index of 3.48 at  $1.06\text{ }\mu\text{m}$ ). Only the polarization of the incident light was varied in the measurements given here, in order to maintain constant polarization of scattered light and hence give the same calibration for the diffraction strength of the blazed gratings in the spectrometer.

The incident-light beam was passed vertically through the sample to match the shape of the scattered-light source to the vertical slits of the spectrometer and eliminate the need for a Dove prism to rotate the orientation of the scattering source in the manner of Mooradian.<sup>12</sup> The Dove prism was avoided after it was found to strongly depolarize the transmitted beam. The spectral response of the scattered light system was carefully calibrated for the polarization corresponding to that of the Raman-scattered light.

#### E. GaAs samples

All our measurements were made on single crystals of  $n$ -GaAs, typically about 0.3-mm cubes and x-ray-oriented within  $2^\circ$ . They were optically polished with a final stage of  $0.05\text{-}\mu\text{m}$   $\gamma$ -alumina powder on microcloth at least on all optically entrant and exit surfaces. The samples were obtained from a variety of sources not all known to us. (We are grateful to R. Sladek and A. Mooradian for some of these samples.)

The carrier concentration information given in Table I was obtained by various means. We specify (1) the values given by the manufacturer or the group from which the material was obtained, (2) the

TABLE I. Specifications of *n*-GaAs samples.

Sample No.	Source	Electron concentration (cm <sup>-3</sup> ) as obtained by various methods		
		As quoted by the source	Hall measurements (Purdue)	Sample resistivity
1	Bell & Howell	$5.9 \times 10^{15}$		$5 \times 10^{15}$
2	Monsanto	$1.6 \times 10^{15}$	$7.4 \times 10^{14}$	$4 \times 10^{14}$
3	Monsanto	$7 \times 10^{14}$	$6.1 \times 10^{14}$	
4	Bell & Howell	$3.8 \times 10^{14}$	$1.9 \times 10^{14}$	
5	Monsanto	$1.5 \times 10^{14}$		$8 \times 10^{12}$
6		$10^{11}$		
7	Bell & Howell	$2.4 \times 10^{16}$		$2 \times 10^{16}$
8	Bell & Howell	$7 \times 10^{16}$		
9	Mooradian			$7 \times 10^{17a}$

<sup>a</sup>Concentration obtained from coupled plasmon-LO-phonon frequency shift.

Hall measurements, where given by the supplier, presumably on samples close to the one used in our measurements, and finally (3) estimates made by us from resistivity measurements on each sample, with the assumption that the mobility was 5000 cm<sup>2</sup>/V sec, a value within a factor less than 2 of the high and low extremes reported in the literature at 300 K. We did not make independent Hall measurements because the samples available were usually too small in size and almost cubic in shape. For such geometry, Hall measurements are notoriously inaccurate (although correctable in theory), and hence were not likely to give any better estimates of the carrier concentration.

#### IV. EXPERIMENTAL RESULTS AND ANALYSIS

The departure of the SPS spectrum from a simple Gaussian line shape has different origins and takes on different forms, depending on (i) the range of carrier concentration considered, and (ii) the particular SPS mechanism or combination of mechanisms governing the scattering process. Our discussion will be divided on the basis of these factors.

##### A. Low carrier concentrations ( $n \lesssim 10^{15}/\text{cm}^3$ ): Competition between SPS and a residual, two-phonon-scattering contribution

A study of samples with progressively lower carrier concentration reveals a significant residual scattering contribution that competes with the scattering from single-particle excitations. This

residual contribution, which occurs in both the  $\hat{e}_i || \hat{e}_s$  and  $\hat{e}_i \perp \hat{e}_s$  scattering configurations, has to be subtracted from the Rayleigh wing in order to obtain the SPS contribution. The details of this residual contribution and its origin are described below.

##### 1. The $\hat{e}_i || \hat{e}_s$ scattering configuration

Figure 4(a) shows a series of SPS spectra for samples 1–4 with electron concentration decreasing from  $5 \times 10^{15}$  to  $2 \times 10^{14}/\text{cm}^3$ . The spectra are shown to scale, with the integrated TO-phonon line in each sample used for normalization. At the highest concentration, the line shape is approximately Gaussian. However, with decreasing carrier concentration a highly structured pattern becomes evident. The details of this pattern and its residual character become more apparent in the magnified plots in Fig. 4(b) for the samples 4–6 extending to still lower concentrations. The structure appears in the same form in every sample, and the spectrum approaches a residual magnitude for  $n \lesssim 2 \times 10^{14}/\text{cm}^3$ . However, for the insulating sample 6, there seems to be an anomalous extra contribution very close to the laser line, associated perhaps with impurities.

##### 2. The $\hat{e}_i \perp \hat{e}_s$ scattering configuration

A very similar, but even more striking manifestation of the residual spectrum is obtained in this configuration. Figure 4(c) shows a series of spectra for samples 2–6, for  $n \lesssim 7 \times 10^{14}/\text{cm}^3$ . The structure is sharper in this configuration. The slight differ-

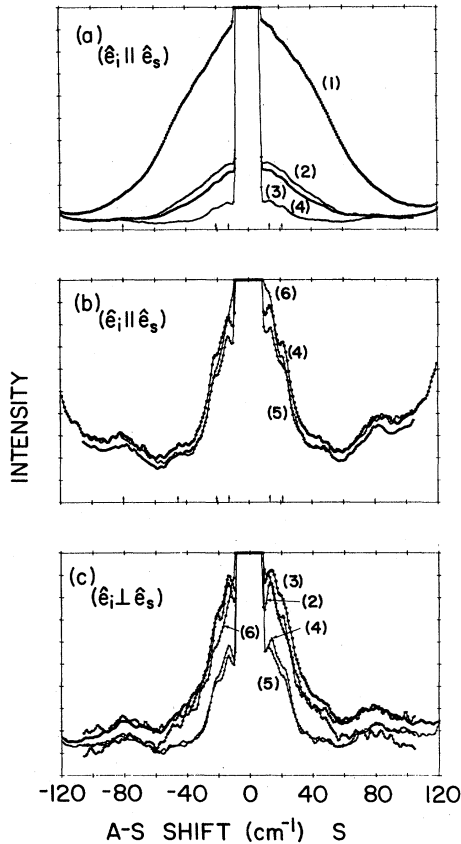


FIG. 4. Spectra showing the appearance of common, residual two-phonon structure as the electron concentration decreases for samples 1–6, varying from  $n=5 \times 10^{15}/\text{cm}^3$  to insulating (see Table I). The two-phonon structure becomes completely dominant for samples 4–6, shown enlarged in (b) and (c). The two-phonon structure is relatively stronger, compared to single-particle scattering, for  $(\hat{e}_i \perp \hat{e}_s)$  in (c). All comparisons between samples are normalized to the TO-phonon line.

ences in height of the spectra are due to the variable free-carrier concentration. Again, the structure is the same in all samples with the exception noted for sample 6.

The fact that the complex, structured scattering contribution has the same form in all samples and appears to have a constant, residual magnitude, indicates that it is not associated with impurities. A comparison with other materials eliminated the possibility that the structure was due to grating ghosts or lines from the krypton pump lamp in the laser. We attribute the structure, i.e., the several peaks and shoulders, to two-phonon-difference scattering involving phonons at the critical points near the Brillouin-zone boundaries.

For confirmation of this interpretation, we cite the following evidence:

(1) In spectra taken at much lower temperature ( $\sim 25$  K), the whole of the structured contribution disappears, leaving only an electronic contribution. Such freezeout is to be expected for two-phonon-difference frequency combinations. Their scattering strength depends on the thermal factor  $(1 + \tilde{n}_1)\tilde{n}_2$ , where  $\tilde{n}_1$  is the occupation number for the phonons emitted and  $\tilde{n}_2$  for the phonons absorbed. Both  $\tilde{n}_1$  and  $\tilde{n}_2$  approach zero at low temperature for phonons with energy  $\hbar\omega \gg k_B T$ .

(2) The various peaks and structures in the two-phonon spectra were identified with the aid of phonon dispersion curves available from neutron scattering measurements for GaAs. Most of the structure is identifiable as two-phonon differences, with some peaks consistent with several possible combinations. The most definitive feature, the sharp peak at  $13.1 \text{ cm}^{-1}$ , is compatible with the combination TO-LO at the  $X$  point.

(3) The symmetry features of the structure were analyzed by obtaining the spectra with  $\Gamma_{15}$  and  $\Gamma_1$  symmetry, by appropriate separation of the contributions from spectra taken in different polarization configurations. It is known<sup>19</sup> that two-phonon combinations (in the present case, difference frequencies involving phonons in different branches) are dominant in  $\Gamma_{15}$  spectra, while overtones (two phonons with the same frequency and opposite wave vector) are dominant in  $\Gamma_1$  spectra. In accord with this, we found that all the structure, and indeed the major portion of the residual contribution, appears in the spectra with  $\Gamma_{15}$  symmetry. That is why the structural features are sharper in the  $\hat{e}_i \perp \hat{e}_s$  spectra which are purely  $\Gamma_{15}$  in character, whereas the  $\hat{e}_i \parallel \hat{e}_s$  spectra contain both  $\Gamma_1$  and  $\Gamma_{15}$  components.

It is evident that a correction for a residual two-phonon contribution is necessary for all samples with carrier concentration  $\lesssim 5 \times 10^{15}/\text{cm}^3$ . The correction was made by first normalizing the data for a given sample to the integrated area of the TO-phonon line, and then subtracting the normalized residual contribution from one of the “purer” samples, 4 or 5. In this operation, the computer storage and manipulation of the data was an essential factor.

A summary of the relative magnitudes of the two-phonon and SPS contributions as a function of carrier concentration is contained in Fig. 5. The curves representing the SPS theory for the two polarization configurations, have been previously presented by Mooradian.<sup>2,8,9</sup> The upper curve is for

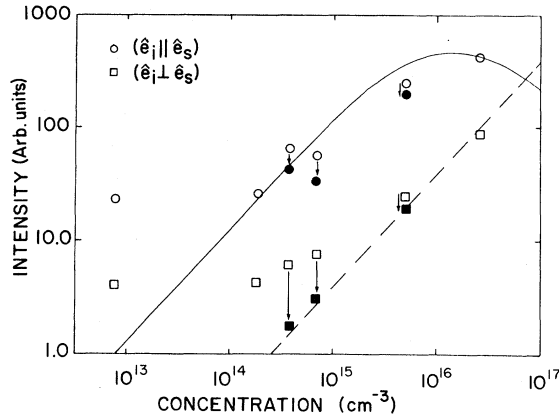


FIG. 5. Plot of integrated area of the spectra as a function of electron concentration for the CDF and SDF mechanisms. Open circles and squares represent the measured data. Data corrected by subtraction of the residual two-phonon-scattering contribution are given by the filled circles and squares.

scattering by CDF, the lower curve by SDF. The latter is weak but gives a linear dependence of scattering cross section on carrier concentration; the former has a limited range of linear response before screening reduces the scattering strength and causes the cross section to peak at  $n \approx 10^{16}/\text{cm}^3$  in GaAs at 300 K. The open data points (circles and squares) represent the directly measured strength of the scattering (the integrated areas of the spectrum for  $|\omega| \leq 100 \text{ cm}^{-1}$ ). The existence of a residual contribution becomes quite obvious. The subtraction of the residual contribution, taken for the sample with  $2 \times 10^{14}/\text{cm}^3$ , gives the closed data points, and tends to restore the expected linear dependence of the SPS on carrier concentration. However, the subtraction is too large to be very reliable for  $n \lesssim 10^{15}/\text{cm}^3$ . A presentation of SPS data similar to that in Fig. 5 was first made by Mooradian.<sup>2,8,9</sup> His data, although much less extensive at low carrier concentration, reveals a similar residual contribution which, however, was not analyzed as such either in the context of that figure nor in its effect on the SPS line shape. It should be noted that while the magnitude of the two-phonon residual contribution depends on the scattering configuration, there is no configuration in which it disappears.

We can proceed now to the presentation of the SPS line shapes, as obtained from the measured data by point-by-point subtraction of the two-phonon residual contribution. The data for sample 2 with  $n = 4 \times 10^{14}/\text{cm}^3$  are shown in Fig. 6(a) for the CDF scattering ( $\hat{e}_i || \hat{e}_s$ ), and in Fig. 6(b) for the

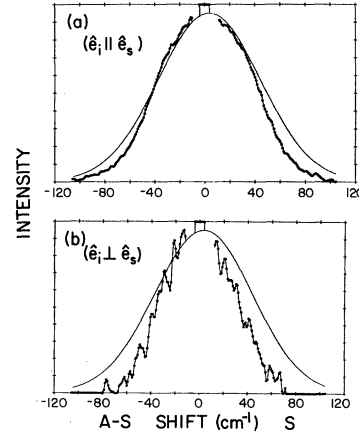


FIG. 6. Comparison of the SPS spectra for  $n = 4 \times 10^{14}/\text{cm}^3$  after the subtraction of the two-phonon contribution, with Gaussian line shape (solid curves). Relative subtraction is much larger for the SDF mechanism ( $\hat{e}_i \perp \hat{e}_s$ ).

SDF scattering ( $\hat{e}_i \perp \hat{e}_s$ ). The solid curves represent simple zero-shift Gaussians at 300 K. At this carrier concentration, the corrections for the two-phonon contribution yields SPS spectra, which are too weak to permit a very accurate analysis of the adequacy of the simple Gaussian approximation. This is especially true for the weak SDF scattering, where the subtracted data is small and noisy. We can do no more than conclude that the simple Gaussian is a *fair* fit here to the SPS line shape. Analysis of the more subtle effects of the approximations in the theory must be left for the samples with higher carrier concentrations and for a special technique discussed in the next section.

#### B. Intermediate carrier concentration: $n = 5 \times 10^{15}/\text{cm}^3$

##### 1. Analysis for the CDF-scattering mechanism

The sole demonstration in the literature of the "fit" of the SPS line shape to a simple Gaussian was for the data of Mooradian<sup>2,8,9</sup> at  $n = 3 \times 10^{15}/\text{cm}^3$ . If we restrict our analysis to the *raw data* for the sample with  $5 \times 10^{15}$  electrons/ $\text{cm}^3$ , we are in good accord with this claim. This can be seen in Fig. 7(a), especially in the range  $|\omega| \leq 100 \text{ cm}^{-1}$ , before the onset of the two-phonon background contributions at the higher-frequency shifts. To obtain a "best-fit" on *both* the Stokes and anti-Stokes sides, it is necessary to include the small zero-shift term ( $\omega_c = \hbar q^2/2m^*$ )

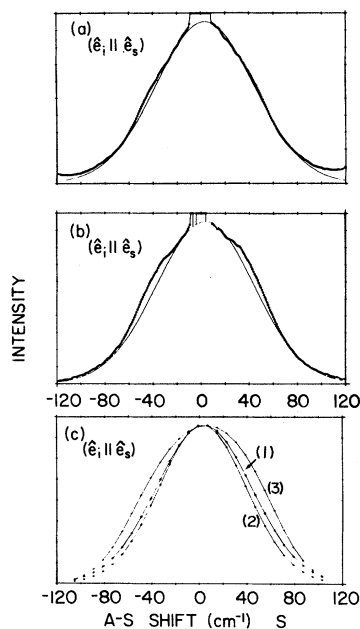


FIG. 7. Analysis of the SPS spectrum for the CDF mechanism for  $n=5 \times 10^{15}/\text{cm}^3$ . (a) Zero-shift Gaussian (solid curve) fits very well to the uncorrected, experimental spectrum. (b) Fit is not as good after subtraction of the small two-phonon contribution. The SPS spectrum then reveals a plasmon bulge and a slight central rise. (c) Theoretical curves 1–3 demonstrate the variations in line shape for different levels of approximation of Eq. (2) (see text).

in the Gaussian. However, further analysis demonstrated that the excellence of the fit is somewhat accidental, and hides several opposing tendencies. First, it is necessary to subtract the small, but not negligible, two-phonon residual contribution. The corrected data in Fig. 7(b) reveal a non-negligible bulging away from the Gaussian curve. This bulging, which becomes much more apparent in samples with higher carrier concentration, represents the onset of the collective-mode, or plasmon, contribution, which is greatly broadened here by Landau damping. A theoretical analysis for this carrier concentration reveals the extent to which the line shape is affected by several compensating factors. Figure 7(c) shows a series of theoretical curves in the collisionless case, all normalized to the same height to better depict transitions in the line shape. Curve 1 represents the simple (shifted) Gaussian. The inclusion of the momentum dependence of the band-structure factor  $A_{\vec{k}}$  inside the integral, but neglecting the screening term in Eq. (2), gives the slightly narrower line shape of curve 2. The effect of the

screening term is to include the Landau-damped plasmon and to broaden the normalized spectrum (curve 3). The effect of the EDF mechanism is small and not shown here. However, we saw in Fig. 1(b) that it can be responsible for the slight rise or peak observed near the laser line. Finally, the effect of collision damping (see Fig. 3), can reduce the plasmon bulge and tend to restore a narrower line shape.

In summary, it is evident that, for this range of carrier concentration, the opposing action of a series of factors, all fairly weak, permits the line shape to be reasonably well approximated by a simple Gaussian form. We have shown that this result is somewhat accidental. We shall see that in most other circumstances, the Gaussian approximation is much less appropriate.

## 2. Analysis for the SDF-scattering mechanism

The SPS data, after correction for the two-phonon residual contribution, are shown in Fig. 8. The experimental line is substantially narrower than the Gaussian (the outer solid curve). It is in reasonably good agreement with the inner theoretical curve, obtained by retaining the  $\vec{k}$  dependence of the band-structure factor  $B_{\vec{k}}$ ; this narrows the halfwidth of the line by about 20%.

## 3. An alternate experimental technique

As a prerequisite to the test of the subtleties in the SPS theory, it was necessary to make a substan-

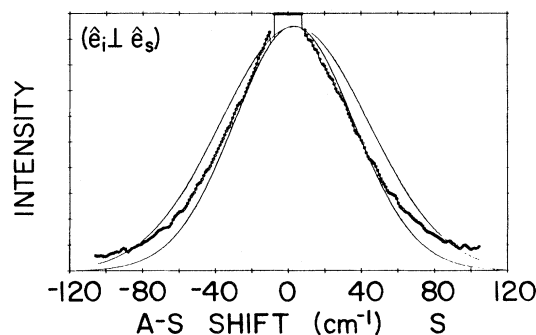


FIG. 8. SPS spectrum for  $n=5 \times 10^{15}/\text{cm}^3$  for the SDF-scattering mechanism after correction for the two-phonon contribution. It is substantially narrower than the zero-shift Gaussian (outer solid curve) and fits well to the theory [Eq. (2)], with the  $\vec{k}$ -dependent factor  $B_{\vec{k}}$  included (inner solid curve).

tial subtraction of the two-phonon spectrum in each sample. The procedure of such subtraction of data on many different samples with different equilibrium concentrations is inherently subject to error due to differences in crystalline orientation and laser-beam alignment, which can affect the magnitude of both the two-phonon and SPS spectra. We have been able to minimize this problem by modulating the carrier concentration on a *single* sample, carrying through the two-phonon subtraction, and observing the progressive changes in SPS line shape.

The modulation of the electron population was found to be possible on all GaAs samples by using intense *Q*-switched Nd:YAlG laser pulses. The same radiation was used for excitation, and for *in situ* 90° Raman scattering. The intense radiation can excite  $\leq 10^{16}$  electrons/cm<sup>3</sup> from deep traps to the conduction band. Such excitation was originally observed in photoconductivity experiments,<sup>20</sup> where it was found to occur even at the lowest light levels and to approach saturation at light intensities of the order of 1 MW/cm<sup>2</sup>. The saturation was attributed to the depletion of the deep traps. The onset of the effect at low intensity indicated that the process did not involve nonlinear (two-photon or second-harmonic) generation. The *Q*-switched measurements were carried out with pulses with halfwidth of 100 nsec and repetition rate of 1000 Hz. A gate of  $\sim 50$  nsec, centered at the peak of the laser pulse, was used in the photon-counting system. The gating was effective in greatly reducing the background due to both dark counts and sample fluorescence. The experiments reported below were made on sample 2 with equilibrium concentration  $n = 4 \times 10^{14}$ /cm<sup>3</sup>. Measurements were made with low-intensity cw laser light and for increasing electron concentration generated by progressively higher *Q*-switched laser intensities. The spectra at the various intensities were normalized to the integrated area of the TO-phonon line for subtraction of the two-phonon (cw) contribution.

A set of corrected SPS spectra for the SDF-scattering mechanism is shown in Fig. 9(a). From the increase in height of the spectra with laser intensity we find an increase in electron concentration of a factor  $\sim 15$ ; thus the data cover a range of  $n$  from  $4 \times 10^{14}$  to  $6 \times 10^{15}$ /cm<sup>3</sup>.

Figure 9(b) shows a repeat of the data, but with the curves normalized to the same height. In spite of the greater fluctuations in the measurements at the lowest pulsed-light intensities, it is evident that the line shapes are very similar and are all substantially narrower than the Gaussian (solid curve) and would fit well the theoretical curve obtained with

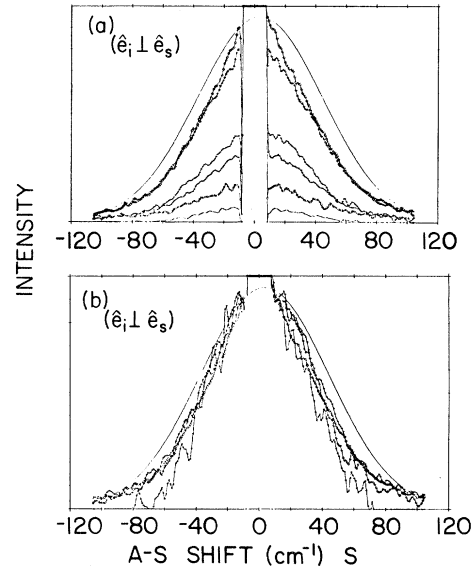


FIG. 9. (a) SPS spectra (corrected for the two-phonon contribution) measured with *Q*-switched radiation pulses of increasing intensity, for the SDF mechanism. Spectra, normalized to the TO-phonon line, show an increase in electron concentration of  $\sim 15\times$  for sample 2. (b) Spectra of (a), normalized to the same height, have a common line shape, narrower than the Gaussian (solid curve), and in good agreement with the  $\vec{k}$ -dependent theory.

the  $\vec{k}$ -dependent band-structure term  $B_{\vec{k}}$ .

From this result we deduce that (1) the laser excitation and modulation of the electron population does not affect its distribution function (as will be discussed further elsewhere), and (2) that the importance of the  $B_{\vec{k}}$  term, demonstrated initially only for the sample with equilibrium concentrations of  $5 \times 10^{15}$ /cm<sup>3</sup>, can now be extended to much lower carrier concentrations. This demonstration is important because as we shall see in the next section, at higher equilibrium carrier concentrations we encounter additional complicating factors which further modify the SPS line shape.

A similar analysis was made for the CDF scattering mechanism for the same sample. Figure 10(a) shows the corrected data for the different light intensities and Fig. 10(b) shows the same data normalized to the same peak height. The Gaussian (solid curve) is included for comparison. In Fig. 10(b) we see that the line shape at low carrier concentrations is close to, but perhaps slightly narrower (as expected) than the Gaussian. With increasing electron concentration, the plasmon bulge develops as expected. The plasmon bulge is similar both for

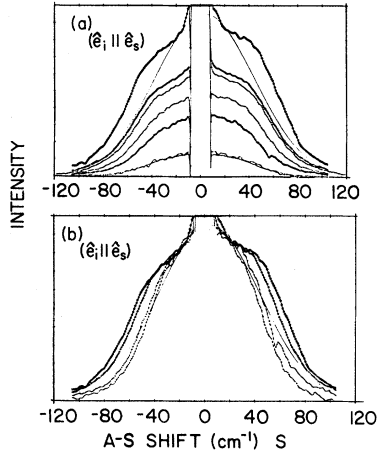


FIG. 10. (a) SPS spectra for sample 2, as a function of  $Q$ -switched incident laser intensity for the CDF mechanism. Spectra are normalized to their respective TO-phonon line, and reflect the increase in electron concentration with increasing laser power. (b) Spectra in (a), normalized to a common height, demonstrate the change in line shape from slightly narrower than the Gaussian (solid curve) to appreciably broader due to the development of the plasmon bulge.

the excited carriers and for an equivalent equilibrium population.

Comparing the evolution of the line shape with changing carrier concentration for the SDF and CDF mechanisms, it is evident that the line shape is well preserved in the former case, but changes considerably in the latter case due to the overlapping effect of the plasmon contribution.

### C. High carrier concentration ( $n \gtrsim 2 \times 10^{16}/\text{cm}^3$ )

#### 1. Analysis for combined effects of the CDF and EDF mechanisms

The evolution of the line shapes for carrier concentrations of  $2 \times 10^{16}$ ,  $7 \times 10^{16}$ , and  $7 \times 10^{17}/\text{cm}^3$  is illustrated for  $(\hat{e}_i || \hat{e}_s)$  in Figs. 11(a), 11(b), and 11(c), respectively. At these carrier concentrations, correction for the two-phonon contribution is no longer necessary. The solid curve in each figure again represents the simple Gaussian. The following features are to be noted:

(i) The plasmon bulge, just beginning to appear at  $n \sim 5 \times 10^{15}/\text{cm}^3$ , grows considerably and causes a drastic broadening of the line shape at  $n = 2 \times 10^{16}/\text{cm}^3$ .

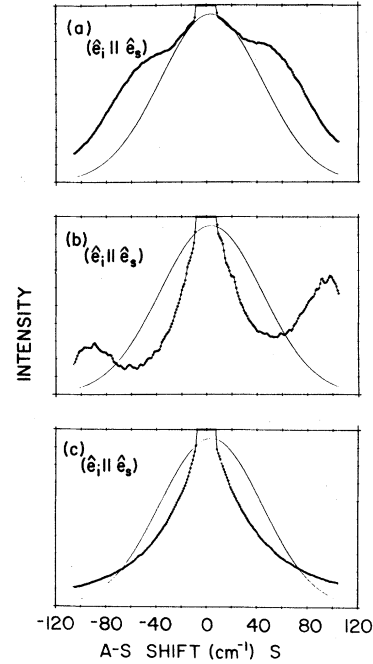


FIG. 11. SPS spectra for the CDF and EDF mechanisms are shown for the increasing carrier concentration in samples 7, 8, and 9, respectively. They demonstrate the evolution of the plasmon contribution, the emergence of the EDF mechanism for the SPS contribution, and the narrowed, Lorentzian line shape for the latter. Zero-shift Gaussian line shapes (solid curves) are shown for reference.

(ii) At progressively higher carrier concentrations, as the plasmon frequency increases, the distinctive plasmon peaks develop in the extremities of the SPS spectrum. At the highest concentration, these peaks lie completely outside the SPS spectrum and outside the range of the plot.

(iii) As the collective modes of the plasma take over, the contribution from single-particle excitations for the CDF mechanisms should be quenched by the increase in screening. However, a central, symmetric peak remains at all carrier concentrations. This peak represents the contribution from the EDF-scattering mechanism which is not screened out and grows with increasing carrier concentration.

(iv) The central peaks at  $n = 7 \times 10^{16}$  and  $7 \times 10^{17}/\text{cm}^3$  deviate considerably from the Gaussian form; the halfwidth is considerably narrowed and the line shape is Lorentzian.

Comparison of the several features described above with the theoretical analysis in Sec. II shows good qualitative agreement. If the observed

plasmon contributions develop more slowly than expected, i.e., if the bulging is weaker and the plasma peaks move out more slowly and grow less rapidly than predicted by the theoretical analysis in Sec. II, this can be attributed to the suppressive function provided by electron collisions.

### 2. Analysis for the SDF-scattering mechanism

Figures 12(a), 12(b), and 12(c) show the SPS spectra for the same set of samples above. The line shapes here are substantially the same in all samples, with a narrowed Lorentzian form similar to that at the higher carrier concentrations in the case discussed above.

### 3. The Lorentzian form of the SPS line shape

In the regime of transition from the CDF- to the EDF-scattering mechanism, and for the SDF-scattering mechanism at  $n \geq 2 \times 10^{16}/\text{cm}^3$ , the SPS spectrum develops a more or less common line shape that is more Lorentzian than Gaussian. The

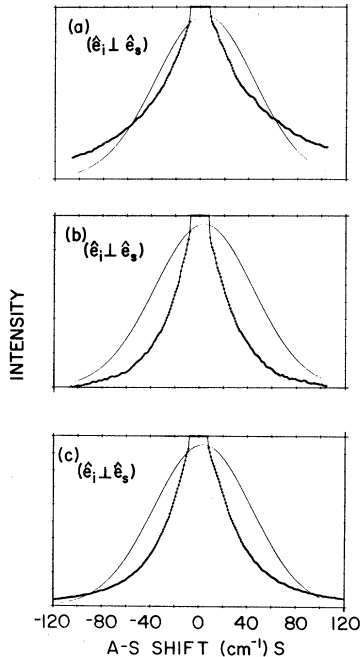


FIG. 12. SPS spectra are shown for the SDF mechanism for increasing carrier concentration in samples 7, 8, and 9, respectively. They demonstrate a similar Lorentzian line shape, much narrower than the Gaussian curves shown for reference, and attributed to short collision times.

theoretical analysis of Hertel and Appel<sup>16</sup> for the CDF-scattering mechanism demonstrates that such an evolution of the line shape can occur for sufficiently short collision times. This result appears to apply for the EDF- and SDF-scattering mechanisms as well. However, we recall the discussion at the end of Sec. II that other complicating factors may begin to affect the line shape just in the regime where the impurity and carrier concentration become large enough ( $> 5 \times 10^{16}/\text{cm}^3$ ) to invoke large collision frequencies.

## V. SUMMARY

We have been concerned with determining to what extent the single-particle-scattering spectrum can be used as a probe of equilibrium or nonequilibrium populations of electrons in semiconductors. We have reassessed the view in much of the original and review literature that the line shape is adequately represented by a Gaussian, and specified several misconceptions and pitfalls that may be encountered in using the single-particle-scattering spectrum as a probe. We summarize the various factors that contribute to complications in the SPS line shape in *n*-GaAs at 300 K as follows:

(1) *Competitive contributions.* At low carrier concentrations, such that  $n \leq 5 \times 10^{15}/\text{cm}^3$ , there is a competitive contribution to the spectrum from two-phonon scattering that must be subtracted to extract the SPS contribution. The two-phonon contribution can be minimized (but not made to disappear) by choosing an appropriate scattering configuration. What constitutes the optimum configuration may not be the same for the CDF- and SDF-scattering mechanisms.

(2) *Scattering mechanisms.* Of the three single-particle-scattering mechanisms, charge-, energy-, and spin-density fluctuations, the latter is the most suitable for probing an electron distribution. It is the only mechanism where the scattering strength is linear with carrier concentration. Its line shape is not complicated by plasmon contributions, which cause bulging of the CDF line shape. The price to be paid for using the SDF mechanism is that it is much the weaker of the two mechanisms.

(3) *Band-structure effects.* Complexities in the energy band structure of the material are responsible for the very existence of the EDF and SDF mechanisms. The band structure further affects the light-scattering cross section through the  $\vec{k}$ -dependent terms in the resonant enhancement fac-



tors,  $A_{\vec{k}}$  and  $B_{\vec{k}}$ . The major consequences for 1.06- $\mu\text{m}$  laser radiation in GaAs at 300 K, are 10% and 20% narrowing of the halfwidths of the line for the CDF and SDF mechanisms. Further small deviations due to nonparabolicity were not included in this analysis. These perturbing effects can be reduced by operating further from the band edge, at the expense of reducing the resonant enhancement of the scattering strength. The effect of strong nonparabolicity *per se*, as in *n*-InSb, have been dealt with separately by Wolff.<sup>11</sup>

(4) *Collisions*. With decreasing collision time, the halfwidth of the single-particle-scattering spectrum narrows, and the nearly Gaussian line shape eventually becomes Lorentzian. Where there is a combination of single-particle and plasmon contributions to the scattering spectrum, collisions broaden and damp the plasmon peaks, until in the limiting case, a Lorentzian line shape is achieved. The combination of single-particle and plasmon scattering occurs only for the CDF mechanism. Its sensitivity to collisions makes it least amenable for analysis of the carrier distribution.

(5) *High carrier concentration*. The SPS line

shape for very high carrier concentrations approaches a common narrowed Lorentzian form, presumably because of the strong impurity scattering. However, the line shape in this regime can also be affected by degeneracy, band-tailing effects due to the impurities, and nonparabolicity.

(6) *Zero shift of the SPS spectrum*. The slight (4- $\text{cm}^{-1}$ ) Compton zero shift of the SPS for *n*-GaAs for 90° scattering is not negligible and has a visible effect on the fit of the theory to the observed line shape at  $n \sim 5 \times 10^{15}/\text{cm}^3$ . With the additional complications at higher carrier concentrations and the transformation in line shape, the zero shift becomes less apparent in both the experimental and theoretically calculated spectra.

#### ACKNOWLEDGMENTS

We are grateful to J. Appel for his interest and for discussions. The work was supported by the National Science Foundation under Grant No. DMR79-14618.

\*Present address: Xerox Wilson Center, Webster, NY 14580.

<sup>1</sup>P. M. Platzman and P. A. Wolff, *Waves and Interactions in Solid State Plasmas* (Academic, New York, 1973).

<sup>2</sup>A. Mooradian, *Raman Spectroscopy of Solids*, in *Laser Handbook*, edited by F. T. Arecchi and E. O. Schulz—du Bois (North-Holland, Amsterdam, 1972), p. 1409; also in *Festkörperprobleme IX*, edited by O. E. Madelung (Pergamon, New York, 1969), p. 74.

<sup>3</sup>M. V. Klein, in *Light Scattering in Solids*, edited by M. Cardona (Springer-Verlag, New York, 1975), p. 147.

<sup>4</sup>Y. Yafet, in *New Developments in Semiconductors*, edited by P. R. Wallace, R. Harris, and M. J. Zuckerman (Noordhoff International, Leiden, 1973), p. 469.

<sup>5</sup>W. Hayes and R. Loudon, *Scattering of Light by Crystals* (Wiley, New York, 1978).

<sup>6</sup>S. S. Jha, *Nuovo Cimento B* **58**, 331 (1969).

<sup>7</sup>D. C. Hamilton and A. L. McWhorter, in *Proceedings of the International Conference on Light Scattering Spectra of Solids*, edited by G. B. Wright (Springer-Verlag, New York, 1969), p. 309.

<sup>8</sup>A. Mooradian, *Phys. Rev. Lett.* **20**, 1102 (1968).

<sup>9</sup>A. Mooradian, in *Proceedings of the International*

*Conference on Light Scattering Spectra of Solids*, Ref. 7, p. 285.

<sup>10</sup>P. A. Wolff, *Phys. Rev. Lett.* **16**, 225 (1966).

<sup>11</sup>P. A. Wolff, in *Proceedings of the International Conference on Light Scattering of Solids*, Ref. 7, p. 273.

<sup>12</sup>A. Mooradian and A. L. McWhorter, in *Proceedings of the Tenth International Conference on the Physics of Semiconductors*, edited by S. P. Keller, J. C. Hensel, and F. Stern (U.S. Atomic Energy Comm., Oak Ridge, Tenn., 1970), p. 380.

<sup>13</sup>R. S. Turtelli, A. R. B. Castro, and R. C. Leite, *Solid State Commun.* **16**, 969 (1975).

<sup>14</sup>E. E. Salpeter, *Phys. Rev.* **120**, 1528 (1960).

<sup>15</sup>D. A. Abramoohn and Ralph Bray, *Bull. Am. Phys. Soc.* **25**, 164 (1980).

<sup>16</sup>P. Hertel and J. Appel, *Phys. Rev. B* **26**, 5730 (1982).

<sup>17</sup>C. Kittel, *Introduction to Solid State Physics*, 5th ed. (Wiley, New York, 1976), p. 223.

<sup>18</sup>R. Loudon, *Adv. Phys.* **13**, 423 (1964).

<sup>19</sup>B. A. Weinstein and M. Cardona, *Phys. Rev. B* **8**, 2795 (1973).

<sup>20</sup>G. K. Celler, S. Mishra, and Ralph Bray, *Appl. Phys. Lett.* **27**, 297 (1975).